Tectonophysics, 202 (1992) 291–308
Elsevier Science Publishers B.V., Amsterdam

The flexural isostatic response of the lithosphere to extensional tectonics

S.S. Egan

Department of Geology, University of Keele, Keele, Staffordshire, ST5 5BG, UK

(Received October 12, 1990; revised version accepted July 2, 1991)

ABSTRACT

Egan, S.S., 1992. The flexural isostatic response of the lithosphere to extensional tectonics. *Tectonophysics*, 202: 291–308.

The tectonic loading resulting from the extension of the lithosphere is examined. Loads resulting from crustal thinning, thermal perturbations and basin infill are recognised and the resulting flexural isostatic deflection of the lithosphere is modelled in response to each of them in the presence of a listric fault. During rifting regional uplift or rebound occurs as a result of both crustal thinning due to normal faulting (simple shear) and the elevation of the geothermal gradient, while subsidence is generated by the downward acting loads created by both basin infill and thinning of the lower crust by stretching (pure shear). Following rifting further flexural subsidence occurs in response to the cooling of the temperature field and associated sedimentary infill.

One of the major tectonic effects, resulting dominantly from crustal thinning by normal faulting, is the generation of footwall uplift. The magnitude of this uplift, along with basin depth and underlying crustal structure, are strongly determined by the flexural rigidity of the lithosphere, the amount of extension and the dip of the major basement fault along which extension is taking place. Depending upon the values of these parameters, model calculations predict between a few tens of metres and 1.5 km of footwall uplift. These values correlate closely with the magnitude of footwall uplift estimated from examples within the geological record. The erosion of this rift induced topography is also proposed as a possible driving mechanism for the generation of major basin unconformities.

1. Introduction

Lithosphere extension or rifting generates a suite of vertical loads, which may vary both laterally and with time. Extension along a major basement fault causes a thinning of the crust, which creates a buoyancy or negative load. The infill of a basin with water and/or sediment generates a positive or downward acting load. In this paper each of these loads are examined to study their effect upon sedimentary basin geometry and underlying crustal structure.

The deflection of the lithosphere in response to a tectonically generated load can be explained by the theory of isostasy, which assumes a depth of compensation (e.g., at the base of the lithosphere) upon and below which the pressures generated by the overlying rock material are everywhere equal. In the simplest case Airy's hypothesis (Airy, 1855) can be used to quantify the isostatic response of the lithosphere to loading. It assumes that following tectonic loading the equality of pressure upon the depth of compensation (i.e. isostatic equilibrium) is maintained by varying the thickness ratio of low-density crust to the denser mantle substratum. A major weakness with Airy isostasy, however, is that it assumes the lithosphere to have no elastic strength with the result that tectonic loading generates uplift or subsidence laterally coincident with the load itself. More realistically, the elastic properties of the lithosphere cause it to flex in response to long-term (greater than 10000 years) loading. The flexural deflection of the lithosphere in response to loading is defined by the theory of flexural or regional isostasy (Walcott, 1970; Turcotte, 1979; Beaumont, 1978, 1981; Watts et al., 1982).

A two-dimensional model of lithosphere extension has been used to define the loading of the lithosphere caused by extensional tectonics

(Kusznir et al., 1987; Egan, 1988; Kusznir and Egan, 1989). The model assumes that extension within the brittle environment of the crust occurs by normal faulting (simple shear), while the lower crust and mantle lithosphere extend by stretching or pure shear. The model has been used to define loads due to crustal thinning by normal faulting and ductile stretching, temperature perturbations and sedimentary infill. The flexural isostatic response of the lithosphere in response to each load has been calculated to give a resultant basement geometry and underlying crustal structure. The model results produce half graben structures with flexurally induced uplift of both the hanging wall and footwall flanks. The sensitivity of these structures to parameters such as the flexural rigidity, the amount of extension and the erosion of subaerial topography have been investigated.

2. The flexural isostatic response of the lithosphere to loading

The flexural isostatic response of the lithosphere (w_x) caused by loading can be modelled by assuming that the lithosphere behaves as a thin elastic plate, which is in equilibrium under the action of all applied loads (e.g. Turcotte and Schubert, 1982):

$$\frac{d^2}{dx^2}D\frac{d^2w_x}{dx^2} + (p_m - p_l)gw_x = L_x \qquad (1)$$

where L_x is the pressure exerted by the applied load, which may vary with the horizontal (x) coordinate, g is acceleration due to gravity, and p_m and p_l are the densities of mantle substratum and load material, respectively. The equation assumes that there is no horizontal force acting parallel to x. D is flexural rigidity, which defines the flexural strength (resistance to bending) of the lithosphere and is given by the following equation:

$$D = \left(ET_e^3\right)/\left[12(1-\upsilon^2)\right] \qquad (2)$$

where E is Young's modulus and υ is Poisson's ratio (see Table 1). T_e represents the effective elastic thickness of the lithosphere and is the most important variable controlling flexural rigidity. It is dependent upon geothermal gradient (Kusznir and Karner, 1985) such that the thickness of the elastic layer is small for high geothermal gradients, resulting in a low flexural rigidity. Alternatively, cool lithosphere has a relatively high effective elastic thickness and, hence, flexural rigidity.

It can be deduced from eqn. 1 that for a flexural rigidity of zero the load is supported entirely by local isostatic restoring forces, whereas for increasing values of flexural rigidity, and hence elastic strength, the load is regionally supported.

TABLE 1

List of symbols

a	thickness of lithosphere	125 km
α	thermal expansion coefficient	3.28×10^{-5} K^{-1}
β_x	extension factor	–
$B_{x,t}$	basin geometry	–
C_o	original crustal thickness	35 km
D	flexural rigidity	–
E	Young's Modulus	70×10^9 Pa
$F_{x,t}$	fault geometry	–
g	acceleration due to gravity	9.81 m s^{-2}
λ	wavelength of load	–
$L_{(x)}$	load function	–
$M_{x,t}$	depth to Moho	–
p_{air}	density of air	0.0
p_c	density of crust	2800 kg m^{-3}
p_l	density of tectonic load	–
p_m	density of mantle material	3300 kg m^{-3}
p_s	density of sediment	2500 kg m^{-3}
P_x	pure shear crustal thinning	–
s	width of load	–
S_x	simple shear crustal thinning	–
t	time	–
ΔT	temperature perturbation	–
T_e	effective elastic thickness	–
T_o	basal lithosphere temperature	1333°C
υ	Poisson's ratio	0.25
w_x	flexural uplift/subsidence	–
x	horizontal co-ordinate	–
Z_d	detachment depth	–

N.B. Values assigned to symbols imply they are constants.

3. Loading caused by extensional tectonics

The dominant load caused by extensional tectonics arises from the thinning of the upper crust by normal faulting (simple shear). Other loads result from the disturbance of the temperature field, ductile deformation of the lower crust, infill

of surface subsidence with water and/or sediment and erosion. The flexural response of the lithosphere to each of these loads are described below in terms of their influence upon sedimentary basin geometry and crustal structure.

3.1. Flexural isostatic effects due to crustal thinning by normal faulting

Large-scale normal faulting causes thinning of the crust (S_x), which can be simulated geometrically (Verrall, 1982; Gibbs, 1983, 1984; White et al., 1986). Crustal thinning imposes a negative load upon the lithosphere and the resulting isostatic uplift ($w_{(s)x}$) is obtained by substituting load and density values into eqn. 1 as follows:

$$\frac{d^2}{dx^2} D \frac{d^2 w_{(s)x}}{dx^2} + (p_m - p_{air}) g w_{(s)x} = -p_c g S_x \quad (3)$$

where p_{air}, p_m and p_c are the densities of air, mantle and crust, respectively (symbols are defined in Table 1). This equation assumes no water or sedimentary infill of resulting surface depressions and that isostatic adjustment is achieved by the upflow of mantle substratum only. This will tend to maximise isostatic deflections because no account is taken of lateral flow within the ductile

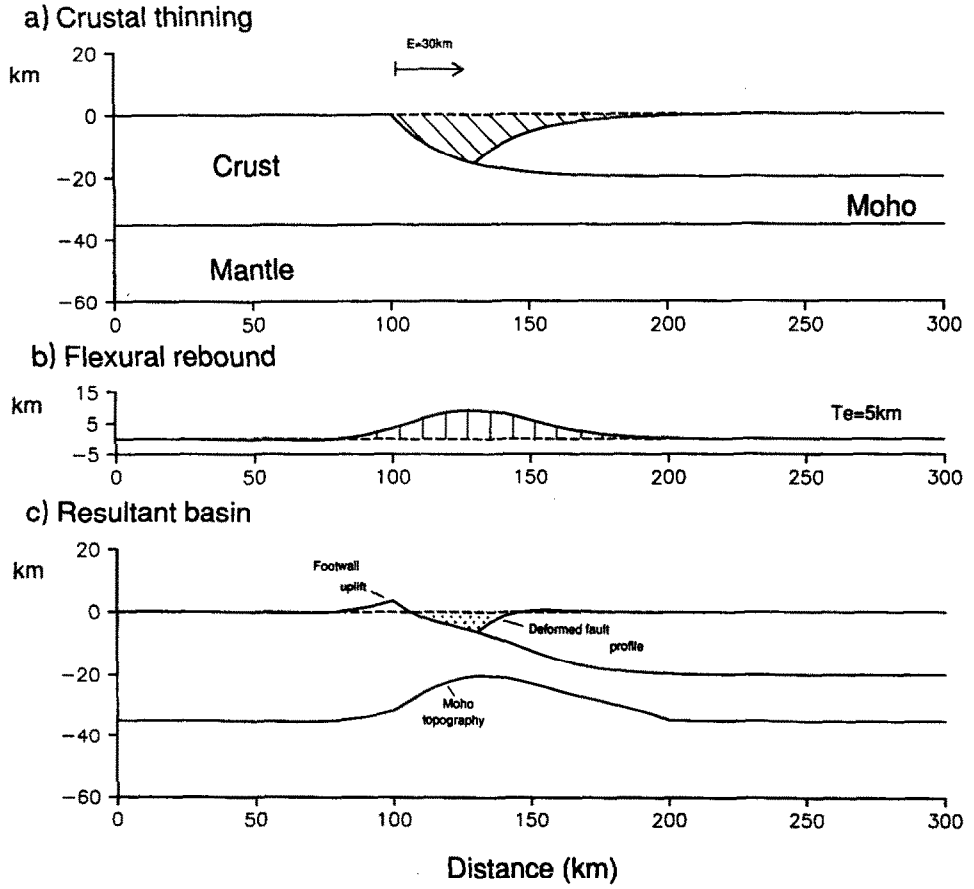

Fig. 1. Simulation of the flexural isostatic response of the lithosphere to 30 km of extension along a major low-angle fault (a). Regional uplift is generated (b), attaining a maximum of approximately 8 km over the basin. This generates a resulting basin some 7 km deep (c) with uplift of both the footwall shoulder and the distal part of the hanging wall. Regional uplift has also caused significant deformation to the original fault geometry (cf. a) along with the generation of a large amount of Moho topography. The calculations for the models have assumed that the flexural rigidity of the lithosphere is defined by an effective elastic thickness of 5 km. Additional tectonically generated load forces, including those arising from thermal effects, basin fill, etc., have been ignored.

environment of the lower crust. There is at present, however, little information on the magnitude of the lateral flow in the lower crust on which to base any modelling work.

In Figure 1a, a listric fault profile (F_x) is shown and is given by:

$$F_x = Z_d[1 - \exp(-x'/Z_d)] \quad (4)$$

where Z_d is the depth at which the fault detaches, which is assumed to be at a depth of 20 km (see section 3.2), and x' is the horizontal distance from the point at which the fault intersects the surface. F_x is assumed to be zero when x' is less than zero.

The Chevron construction (Verall, 1982; Gibbs, 1983, 1984) has been applied to determine the distribution of crustal thinning (S_x) produced by extension along this fault such that:

$$S_x = F_x - F_{(x-E)} \quad (5)$$

where E is the amount of extension (heave). The calculations presented in Figure 1a assume 30 km of extension, which, although unrealistically large when compared to real geological examples of normal faulting along basement faults, has been used to clarify the subsequent flexural isostatic adjustment.

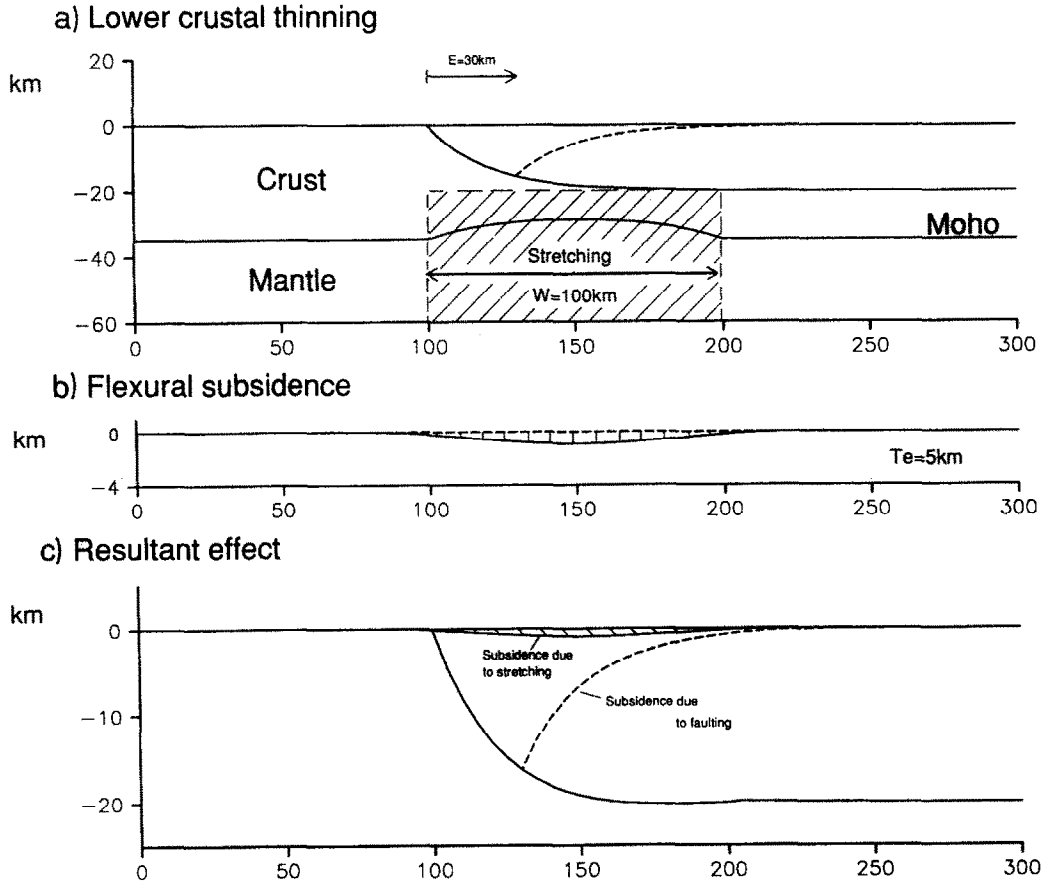

Fig. 2. Evidence from deep seismic reflection data and strength studies of the lithosphere show that extension within the upper crust is achieved by normal faulting (simple shear), while the ductile environment within the lower crust and mantle lithosphere extends by a stretching mechanism (pure shear). (a) Stretching is assumed to occur below an intracrustal detachment depth of 20 km and has been distributed over a width of 100 km. In order to avoid mass balance problems the total amount of pure shear deformation balances 30 km of extension by simple shear. (b) Stretching causes a thinning of the lower crust. Isostatic restoring forces cause a replacement of the removed crustal material by denser mantle—regional subsidence results. (c) Superposition of the flexing profile generated by the pure shear deformation upon the original surface depression enhances surface subsidence.

Equation 3 has been solved numerically, as described in the Appendix, to calculate the pattern of flexural uplift (Figure 1b). The superposition of this profile upon the original surface depression (Figure 1a) generates a basin geometry and crustal structure as shown in Figure 1c. Modifications to the original surface depression include a reduced basin depth, footwall uplift, deformation of the listric fault profile and the generation of a substantial amount of Moho topography. These effects are further discussed in section 4.

3.2. *Flexural isostatic effects due to ductile extension in the lower crust and mantle lithosphere*

Seismic reflection evidence shows that major extensional faults are restricted to relatively shallow depths (e.g., Hall et al., 1984; BIRPS and ECORS, 1986) and that these faults mainly flatten or detach in the ductile environment of the mid crust (Jackson and McKenzie, 1983; Kusznir and Park, 1987; Kusznir et al., 1987). In this ductile region extension is assumed to occur by a regionally distributed stretching or pure shear mechanism (McKenzie, 1978).

In Figure 2, the major basement fault is assumed to detach into a mid-crustal detachment zone at a depth of 20 km, below which extension occurs by pure shear. The thinning of the lower crust causes the Moho and underlying dense mantle material to rise (Figure 2a). The amount of crustal thinning by pure shear (P_x) is given by:

$$P_x = (C_o - Z_d)(1 - 1/\beta_x) \tag{6}$$

where C_o is original crustal thickness, Z_d is the detachment depth of the overlying fault and β_x is the extension factor (McKenzie, 1978).

It is assumed that extension by faulting and pure shear balance in order to avoid mass balance problems. Due to the ductile nature of the lower crust, however, the pure shear extension is regionally distributed relative to the localised faulting above. β_x is assigned a sinusoidal distribution such that:

$$\beta_x = \beta' \sin(\pi x/W) + 1 \tag{7}$$

where W is the width over which the pure shear is distributed and $\beta' + 1$ is the maximum extension factor such that:

$$\beta' = (\pi/2)[E/(W - E)] \tag{8}$$

where E is the amount of fault-controlled extension (heave).

The resulting flexural subsidence ($w_{(p)x}$) profile (Figure 2b) has been calculated from:

$$\frac{d^2}{dx^2} D \frac{d^2 w_{(p)x}}{dx^2} + (\rho_m - \rho_{air}) g w_{(p)x} = (\rho_m - \rho_c) g P_x \tag{9}$$

A fuller description of the modelling of pure shear extension in the lower crust and mantle lithosphere can be found in Kusznir et al. (1987) and Kusznir and Egan (1989).

3.3. *Flexural isostatic effects due to temperature field disturbances*

Rifting perturbs the lithosphere temperature field. Normal movement along major basement faults juxtaposes cool hanging-wall rock against that of the hotter footwall, thus generating a temperature discontinuity across the fault. Pure shear, beneath the horizontal detachment, thins the lithosphere so that deep rocks are moved to a shallower depth. The resulting thermal expansion produces uplift of the surface (McKenzie, 1978). Following rifting the isotherms within the lithosphere cool back to an equilibrium state with a time constant of the order of 100 Ma. The associated thermal contraction generates the thermal subsidence phase apparent in the stratigraphic histories of many extensional sedimentary basins.

The flexural isostatic response of the lithosphere ($w_{(th)x,t}$) to the thermal perturbations can be calculated at any point in time from the following equation:

$$\frac{d^2}{dx^2} D \frac{d^2 w_{(th)x,t}}{dx^2} + (\rho_m g w_{(th)x,t}) = \int_0^a \alpha \, \Delta T \rho' g \, dz \tag{10}$$

where ΔT is the temperature perturbation, α is the coefficient of thermal expansion, a is lithosphere thickness and ρ' is density, which is de-

pendent upon the depth (all symbols are defined in Table 1). There are several documented methods for calculating the rift-induced perturbation of the temperature field. For example, McKenzie (1978) calculates the temperature disturbances by assuming that lithosphere extension occurs by pure shear deformation only, while Kusznir and Egan (1989) take into account both crustal faulting and pure shear deformation in the lower crust and mantle lithosphere when modelling the temperature field disturbances. This latter, more realistic, methodology has been used for the modelling described here. The model calculations assume a simple initial steady-state geotherm ($T_{x,z}$), prior to extension, to be given by:

$$T_{x,z} = (z/a)T_0 \tag{11}$$

where a is lithosphere thickness, z is depth and T_0 is the temperature at the base of the lithosphere.

The re-equilibration of the temperature field following rifting can be calculated numerically by assuming that the lithosphere cools by gradual heat loss due to conduction:

$$\frac{dT}{dt} = \frac{k}{p\sigma}\left(\frac{d^2T}{dx^2} + \frac{d^2T}{dz^2}\right) \tag{12}$$

where T is temperature, t is time, k is thermal conductivity, σ is specific heat and p is density.

Equation 12 has been solved numerically using the finite-difference method (e.g., Egan, 1988). The boundary conditions of 0 and 1333°C have been used to represent the surface and base of the lithosphere, respectively.

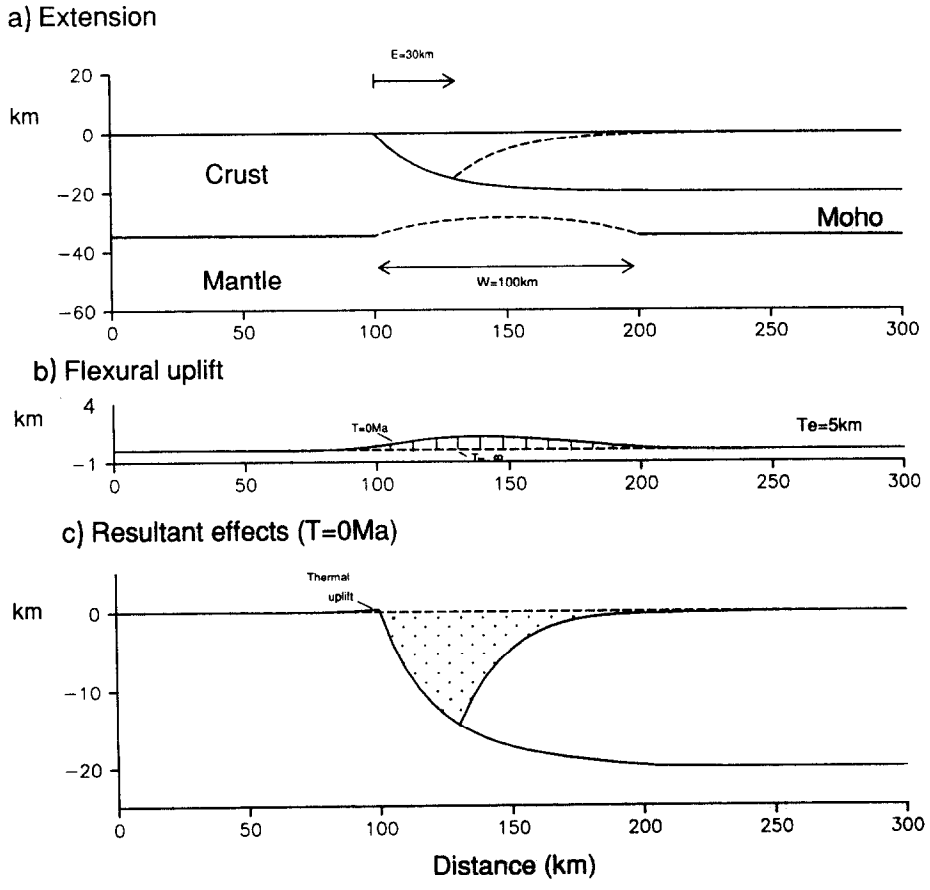

Fig. 3. Both normal faulting and stretching (a) raise hotter material at depth nearer to the surface. The isostatic effect of this increased geothermal gradient is to generate a regional uplift profile (b). This reduces subsidence within the original fault-induced basin and causes uplift of the footwall shoulder by about 400 m. These effects are gradually removed, however, over a time interval of about 100 Ma in response to lithosphere cooling.

In Figure 3b, the uplift profile arising from the thermal perturbations following 30 km of extension along a listric fault are shown. Extension in the lower lithosphere has been positioned beneath the basin and distributed over a width of 100 km (Figure 3a). Initially, the uplift decreases the overall subsidence in the basin and raises the footwall shoulder by approximately 400 m (Figure 3c). Following rifting, however, the raised temperatures re-equilibrate and the basin subsides back to its original position, in the absence of erosion or other loads.

3.4. The flexural effects due to infilling a basin

Once a basin forms it rarely remains starved of infill material. In many cases, particularly at those passive margins where sediment supply is abundant, infill by sediment is rapid enough to keep pace with fault-induced subsidence. The infilling material acts as a downward acting load upon the lithosphere inducing further subsidence as shown in Figure 4a, where sediment loading has been assumed to occur to sea level. The flexural isostatic subsidence, $w_{(i)x}$, resulting from basin fill can be calculated from the following equation:

$$\frac{d^2}{dx^2} D \frac{d^2 w_{(i)x}}{dx^2} + \left[(p_m - p_i) g w_{(i)x} \right] = B_{x,t} p_i g \tag{13}$$

where $B_{x,t}$ defines the basin depth to be infilled with material of density p_i.

An infill density of 2500 kg m^{-3} has been assumed in the calculations. This was judged to

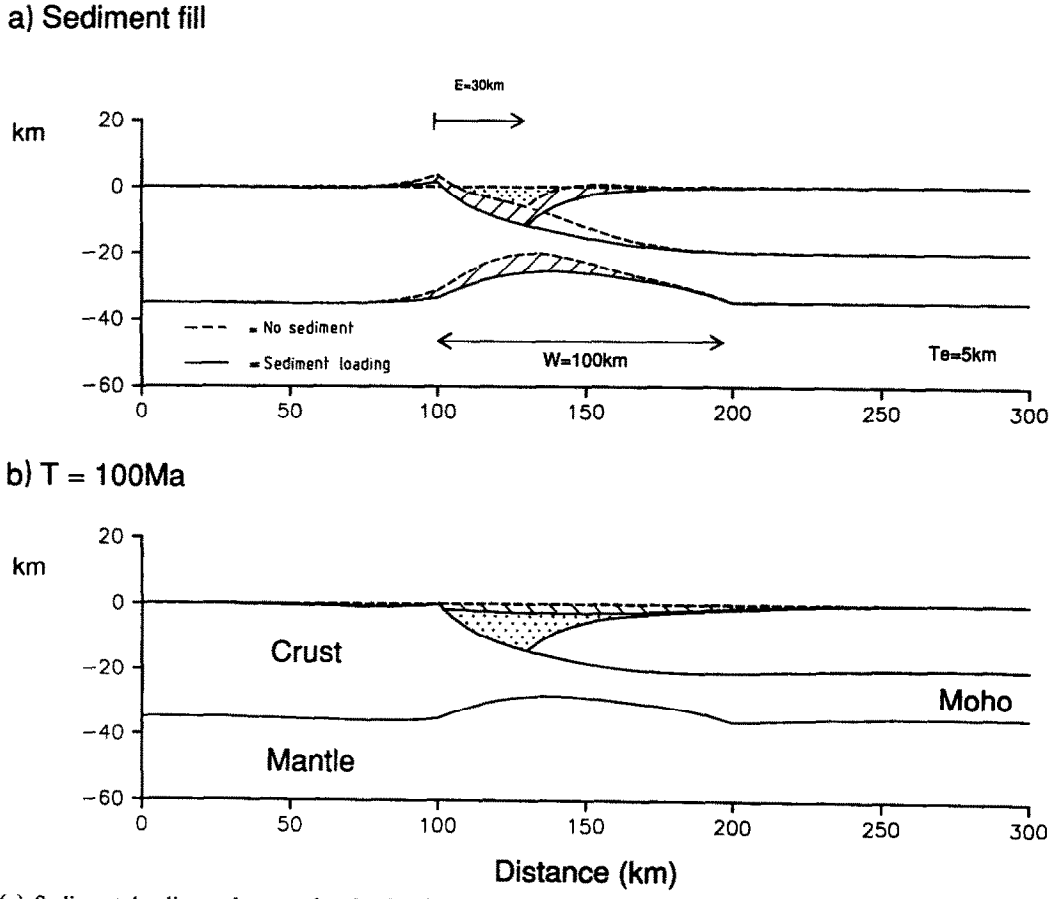

Fig. 4. (a) Sediment loading enhances the depth of the basin and reduces the magnitude of both footwall uplift and Moho topography as well as producing a smooth fault geometry. (b) Cooling of the lithosphere following rifting creates further subsidence which is amplified by sediment infill. The model shows a sedimentary sequence within the basin consisting of a rift component (dotted ornament) overlain by a broad, thin blanket of thermally induced deposition (shaded ornament).

be a sound average taking into account that the sediment at the top of the basin would have a relatively low density of around 2100 kg m^{-3}, while the initial infilling material at the bottom of the basin will have been compacted almost to a crustal density of 2800 kg m^{-3}. The load is time dependent because of the effects of the post-rift cooling of the temperature field, which generates additional subsidence over time. It should be noted that eqn. 13 only yields approximate values for the flexural subsidence generated by loading from basin fill because it assumes a constant density contrast of $p_m - p_i$ across both basin and flanking regions. This will exaggerate, in particular, the amount of uplift of the footwall shoulder. A more accurate, iterative method of calculating the flexural subsidence arising from basin infill is described by Watts et al. (1982) and by Egan (1988).

In Figure 4b basin geometry and crustal structure are shown for 100 Ma following 30 km of instantaneous rifting along a listric fault. The results show the combined effect of each of the loads described above as well as the enhanced subsidence caused by sediment loading to sea level throughout all phases of basin evolution. The dotted ornament represents subsidence arising from rifting, while the shaded ornament defines the thermal subsidence component.

Basement elevation relative to sea level ($B_{x,t}$) is represented at any point in time by the following equation:

$$B_{x,t} = S_x + W_{(s)x} + W_{(p)x} + W_{(th)x,t} + W_{(i)x,t} \quad (14)$$

while Moho depth is given by:

$$M_{x,t} = C_o - S_x - P_x + B_{x,t} \quad (15)$$

where C_o is the original crustal thickness.

Fault geometry is given by:

$$F_{x,t} = M_{x,t} - (C_o - F'_x - P_x) \quad (16)$$

where F'_x is the pre-extensional fault profile.

4. The flexural isostatic control upon the magnitude of footwall uplift and basin depth

There are several mechanisms proposed to explain the origin of footwall uplift following extensional tectonics. One possibility is the lateral flow of heat from beneath the basin into flanking regions (Cochran, 1983). Although this mechanism must apply, such thermal perturbations are temporary on a geological time scale and thus are inconsistent with permanent footwall uplift. Another mechanism attributes footwall uplift to regional thinning of the mantle lithosphere in relation to localised thinning of the crust (Royden and Keen, 1980; Hellinger and Sclater, 1983; White and McKenzie, 1988). This mechanism would also only induce a temporary uplift. Another major problem with both these mechanisms is that the magnitude of the footwall uplift produced would be very small. Figure 3b shows that the thermally induced uplift over a basin produced by 30 km extension is only about 1 km. At the basin flanks the flexural deflection diminishes to approximately 400 m and sediment loading would reduce this further. Footwall uplift, however, of between 500 m and over 1 km have been recognised for relatively small, more realistic, amounts of extension (Weissel and Karner, 1989; Yielding, 1990). These observations discount a thermal origin as being the main cause of footwall uplift.

A more viable mechanism to explain the origin of footwall uplift following extension is the flexural isostatic response of the lithosphere in response to large-scale normal faulting as described in section 3.1. The flexural isostatic forces arising due to lithosphere extension are both prolonged over geological time and of sufficient magnitude to induce topography several hundred metres or more in height.

The magnitude of footwall uplift resulting from extension is dependent upon the amount of fault-controlled extension, and hence crustal thinning, as well as the flexural rigidity of the lithosphere. The effect of these parameters along with that of the dip of the extensional fault are examined in the following sections.

4.1. The effect of the amount of extension upon the magnitude of footwall uplift

In Figure 5, the maximum height of footwall uplift above sea level has been plotted against

increasing extension along a listric fault, detaching at a depth of 20 km, for flexural rigidities defined by elastic thicknesses of 5, 15 and 30 km, respectively. The footwall uplift results from the flexural response of the lithosphere to fault-induced crustal thinning (simple shear). Extension in the lower lithosphere, thermal effects and sediment loading are ignored in Figure 5a, whereas these loads have been included in Figure 5b, causing the height of footwall uplift to be reduced to more realistic values due to subsidence arising from lower crustal thinning and sediment infill. Initially, footwall uplift gradually increases with increasing extension for all three values of flexural rigidity and then stabiles. For example, it can be seen in Figure 5a that for an elastic thickness of 5 km the footwall uplift rises to a maximum of 3.5 km at an extension of 30 km, after which it stabilises. An elastic thickness of 15 km generates a maximum footwall uplift of 5.7 km at an extension of 60 km before it stabilises, however, extensions of this magnitude along single fault structures are not apparent in the geological record.

4.2. The effect of increasing flexural rigidity upon footwall uplift and basin depth

In Figure 6, flexural uplift profiles are plotted for elastic thicknesses of 5 and 30 km, respec-

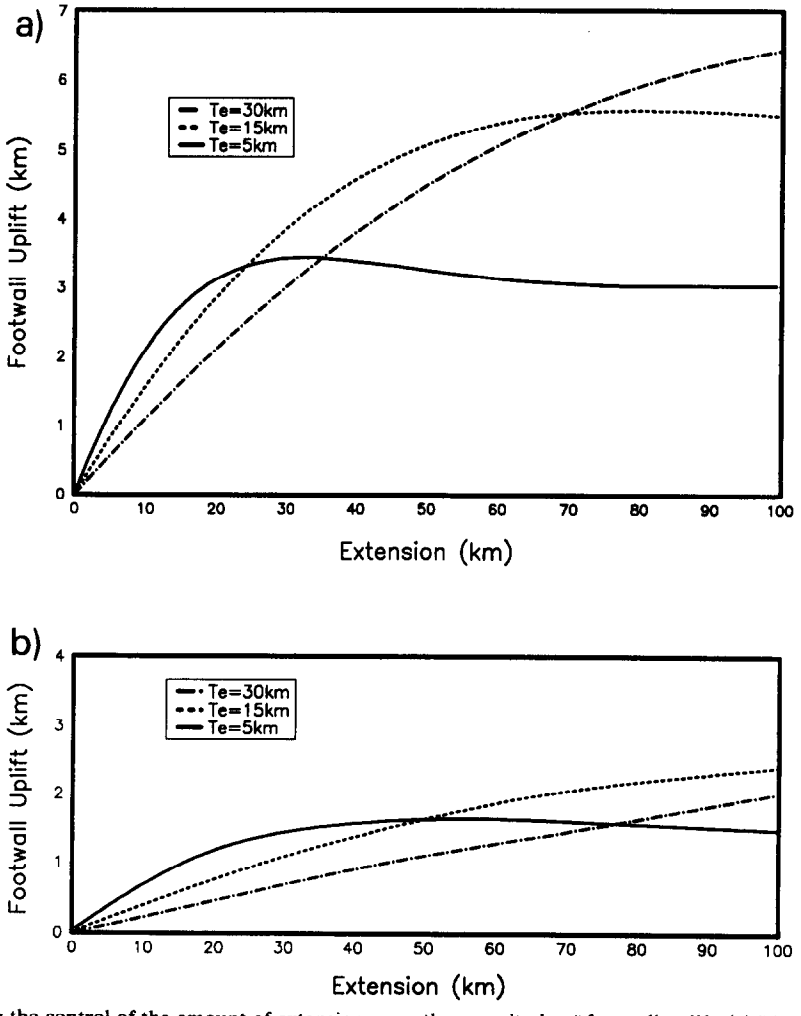

Fig. 5. Graphs showing the control of the amount of extension upon the magnitude of footwall uplift. (a) The flexural effects arising from crustal thinning by simple shear. (b) Flexural effects arising from crustal thinning due to both simple and pure shear, thermal perturbations and sediment infill to sea level have been considered.

tively, for an extension of 50 km along a listric fault. Although the greatest amount of uplift is generated for the smaller flexural rigidity the width of the flexural profile at this value is relatively small so that the high rebound over the load (the basin) is only partially transferred onto the footwall shoulder. An elastic thickness of 30 km generates a smaller maximum uplift over the load, but the uplift extends more effectively over the basin peripheries.

The results presented in Figure 6 are further clarified by those in Figure 7. Figure 7a shows a maximum footwall uplift plotted against elastic thickness for extensions of 10, 30 and 50 km, respectively, along a listric fault with a surface dip of 45°. The lithosphere has no flexural strength for an elastic thickness of zero and, hence, no footwall uplift results. As flexural rigidity increases the height of the uplift of the footwall shoulder begins to increase sharply and then gradually decreases again to zero for the hypothetical situation of an elastic thickness of infinity. For example, an extension of 30 km generates a maximum footwall uplift height of about 4 km for an elastic thickness of 10 km. For low values of flexural rigidity the lithosphere has a high rebound capacity in response to crustal thinning. At an elastic thickness of 50 km the height of the footwall topography has dropped to approximately 2.5 km showing the low rebound capacity of the lithosphere at high values of flexural rigidity. Despite the reduced height of footwall topog-

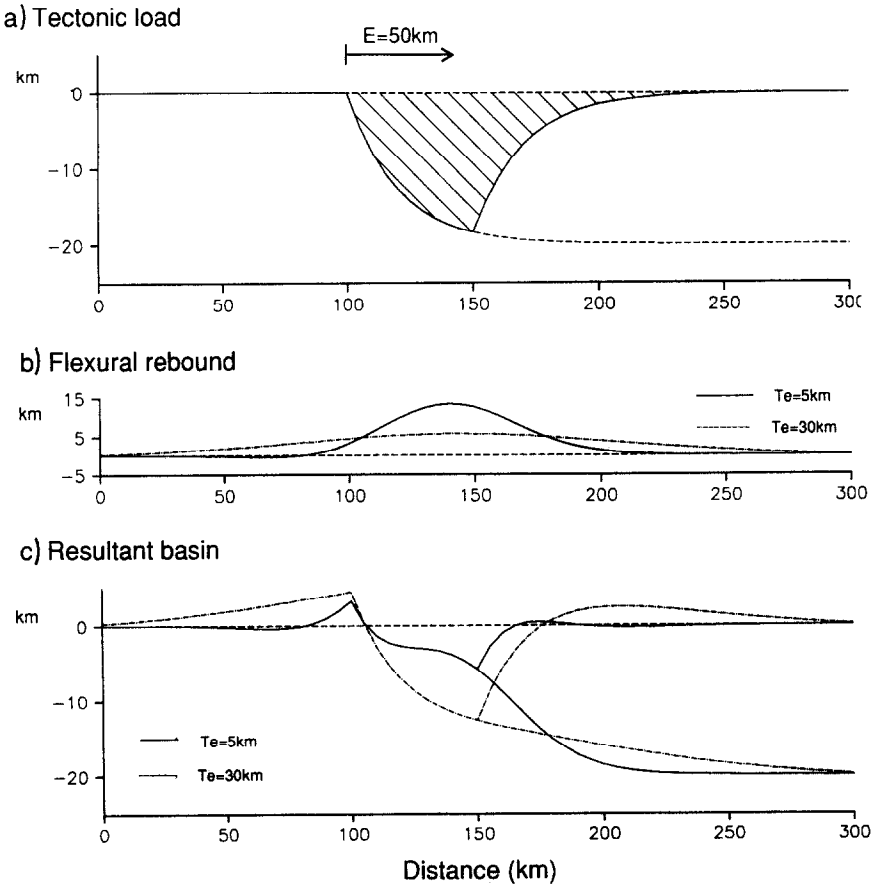

Fig. 6. The height and width of the flexural uplift profile arising from 50 km of extension (a) is controlled by the flexural rigidity of the lithosphere. A low flexural rigidity (e.g., as defined by $T_e = 5$ km) generates a large amount of flexural uplift over the basin, which is relatively confined in lateral extent (b). A large flexural rigidity (e.g., as defined by $T_e = 30$ km) generates a relatively low amount of uplift over the basin, but which is more regionally dispersed. It follows that the resulting flexurally compensated basin geometry is strongly influenced by the flexural rigidity of the lithosphere (c).

raphy generated for high values of flexural rigidity, the lateral extent of the uplift is gradually widened as flexural deflections are dispersed over an increasing width (Fig. 7b).

In Figure 7c, maximum basin depth has been plotted against elastic thickness and shows a basin deepening with increasing flexural rigidity. Airy isostasy ($T_e = 0$) allows maximum uplift to occur in response to crustal thinning and a relatively shallow basin results. As the flexural strength increases, the isostatic uplift is reduced at any point within the basin, resulting in an increased

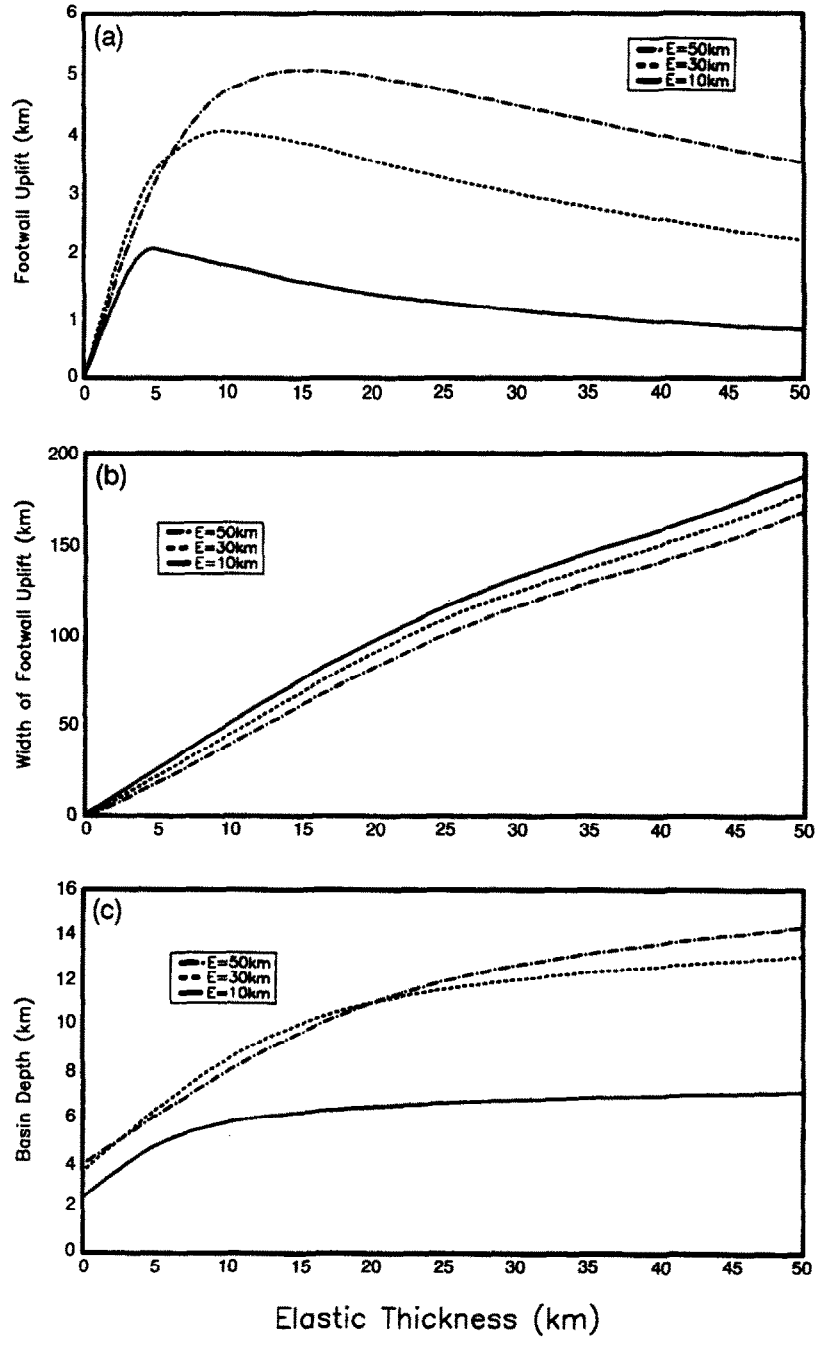

Fig. 7. The control of flexural rigidity, as defined by elastic thickness, upon the height (a) and width (b) of footwall uplift, and basin depth (c). Only the flexural effects occurring in response to crustal thinning by simple shear have been considered.

basin depth. The results also have important implications for explaining the amount of Moho topography generated following extension. Low values of elastic thickness cause a relatively large amount of flexural uplift, bringing the Moho relatively near to the surface. As flexural rigidity increases, however, the amount of associated flexural uplift decreases and a subdued Moho topography is produced.

4.3. The effect of fault dip on the magnitude of footwall uplift

The angle of dip of the fault controls the geometry of the surface depression created by simple shear extension. A steep fault generates a strongly asymmetric buoyancy load, and as a result the height of footwall uplift is increased. Figure 8 shows flexural rebound profiles calculated for 30 km extension along faults with surface dips of 30°, 45° and 60°. The amount of flexural rebound is greatest for the fault dipping at 60°, which reflects the strongly asymmetric and deeper surface depression created by normal faulting.

5. The flexural origin of major unconformities

It has already been demonstrated that footwall uplift results from the flexural isostatic rebound of the lithosphere in response to normal faulting (Figure 9a). Footwall uplift is rarely preserved in

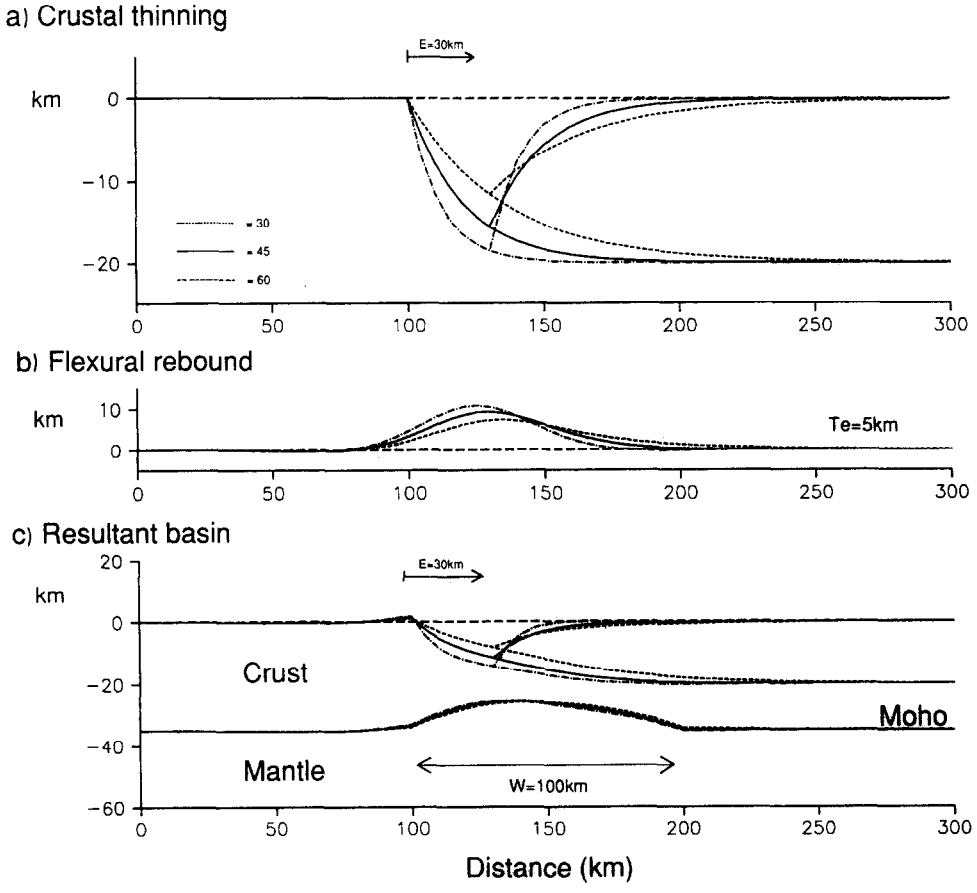

Fig. 8. (a) 30 km of extension along faults dipping at 30°, 45° and 60°, respectively. A steepening of the fault generates a deepening and narrowing of the surface depression. (b) The associated flexural uplift profiles show a gradual increase in the amount of uplift over the basin in response to an increasing fault dip. The rebound profile is noticeably asymmetric towards the footwall for the 60° profile. (c) The resultant basement geometries and crustal structures show that increasing the fault dip both deepens and decreases the width of the basin, while the magnitude of both the footwall uplift and Moho topography are increased by a small amount.

the geological record, however, due to the effects of erosion. Yielding (1990), for example, describes the extensive erosion of footwall uplift, caused by Jurassic normal faulting, in the northern North Sea. It is proposed here that the erosion of footwall uplift imposes a negative load upon the lithosphere, which causes a more widely dispersed isostatic uplift. The amount of uplift ($w_{(er)x}$) generated by the erosion of approximately 1.5 km of footwall uplift is shown in Figure 9b and has been calculated from:

$$\frac{d^2}{dx^2}D\frac{d^2w_{(er)x}}{dx^2} + (p_m - p_{air})gw_{(er)x} = p_c g U_{(x,t=0)} \quad (17)$$

where $U_{(x,t=0)}$ is the magnitude of the eroded uplift.

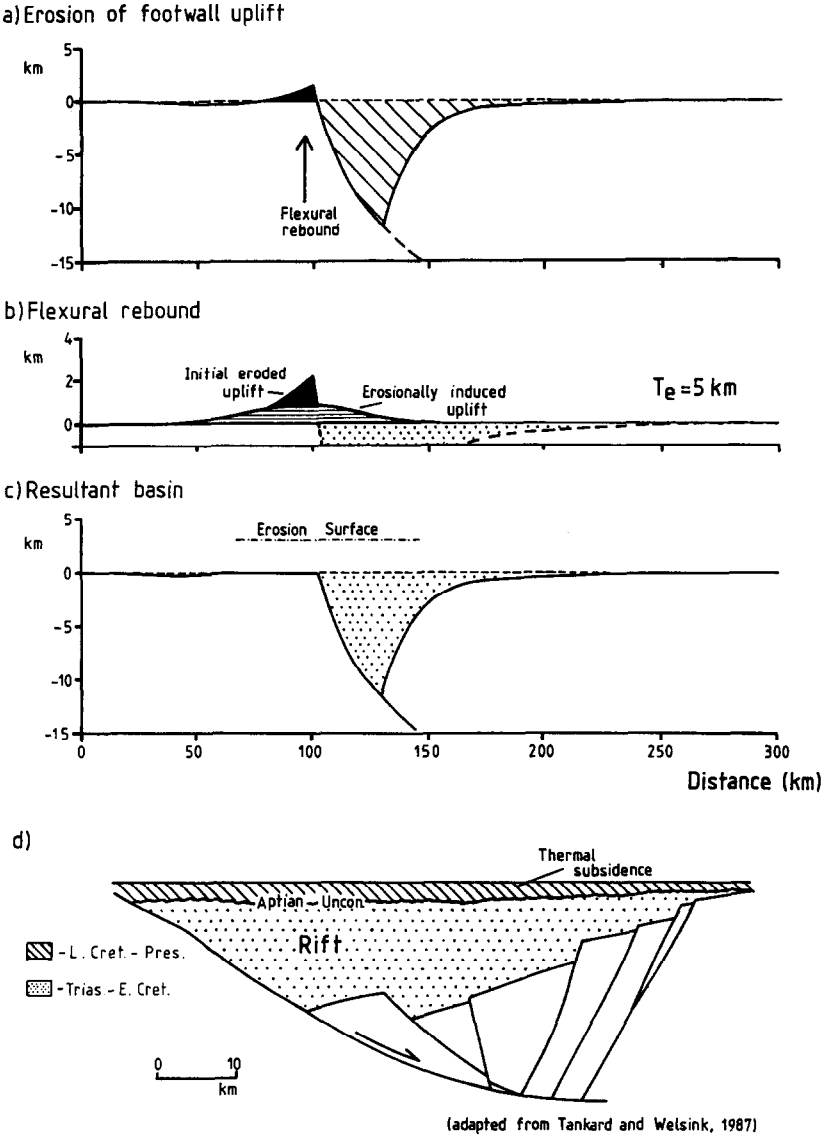

Fig. 9. The flexural response of the lithosphere to extension by simple shear generates footwall uplift (a). Erosion of this uplift constitutes a thinning of the crust and causes more flexural rebound (b). The process is capable of generating an erosion surface across the basin (c). This mechanism may explain the origin of major unconformities, which separate rift and thermal subsidence deposition, in many major extensional basins, such as the Jeanne d'Arc basin of Grand Banks, Newfoundland (d).

Further erosion of this new uplift ($W_{(er)x}$) generates an erosion surface, which is capable of extending across most of the basin (Fig. 9c). The process may explain, therefore, the occurrence of major ("breakup") unconformities, separating rift from thermal subsidence depositional sequences within major extensional sedimentary basins. For example, the Aptain unconformity within the sedimentary sequence of the Jeanne d'Arc basin in Grand Banks region of Newfoundland (Fig. 9d) separates Triassic to Early Cretaceous rift sequences from the subsequent thermal subsidence phase, which began in the Late Cretaceous (Enachescu, 1987; Tankard and Welsink, 1987; Tankard et al., 1989). Seismic reflection data across the basin (Keen et al., 1987) reveals an absence of footwall uplift, implying that it was quickly eroded. It is suggested that this erosion induced regional uplift, and, in turn, an erosion surface across the whole basin before the onset of thermal subsidence.

The flexural isostatic implications of large-scale erosion are discussed in more detail in Egan (1988), while Couzens and Kusznir (more known) investigate the validity of the mechanism for explaining the origin of "breakup" unconformities.

6. Discussion

It has been shown that the flexural isostatic response of the lithosphere to the loading generated by extensional tectonics has an important influence upon sedimentary basin geometry and underlying crustal structure. The results show that the flexural isostatic response of the lithosphere must be considered if phenomena such as footwall uplift are to be explained. The flexural origin of the uplift of the footwall shoulder was first recognised and formulated by Vening Meinesz (1950) from investigations he was conducting on the East African rift system. He suggested that following extension along normal faults the hanging wall flexurally subsides to form a rift valley, while the footwall rises due to elastic upbending (see also Heiskanen and Vening Meinesz, 1958; Bott, 1976; Jackson and McKenzie, 1983). The Vening Meinesz theory can be criticised for being limited in application as it assumes that the dip of the fault along which extension is taking place to be the main controlling parameter on the flexural behaviour of the footwall and hanging-wall blocks. The methodology has also been criticised by Jackson and McKenzie (1983) for yielding approximate predictions for the effects of asymmetric loads and by Weissel and Karner (1989) for being speculative about the interaction between the faulted blocks during extension. The modelling methods described here assume that the footwall and hanging wall remain in contact following rifting so that the lithosphere can be assumed to behave as a single, unbroken elastic plate during isostatic adjustment. This assumption is not valied over the co-seismic time scale (0.1 to 1 Ma after fault movement) when vertical displacements between the hanging wall and footwall blocks are consistent with an elastic dislocation process (King et al., 1988). The modelling is applicable, therefore, to non-active fault systems where the co-seismic elastic bending stresses and associated displacements have been gradually relieved by creep within the lower crust and mantle so that basement geometry is determined by co-seismic fault displacement and post-seismic flexural isostatic adjustment.

The magnitudes of footwall uplift, basin depth and Moho topography generated following rifting have been shown to be dependent upon the amount of extension, the fault dip and the flexural rigidity of the lithosphere. Model results show footwall topographies of between 0 and 2.5 km can be generated for realistic amounts of extension, depending upon the value of flexural rigidity used (Fig. 5b). The amount of footwall uplift can be determined more specifically, therefore, by attempting to determine the effective elastic thickness, and hence flexural rigidity, of the lithosphere at the time of rifting. Numerical modelling of the evolution of the Viking Graben in the northern North Sea (Marsden et al., 1990) shows that models incorporating elastic thickness values of 6 and 3 km for Triassic and Jurassic rift phases most closely predict the observed basin subsidence. Similar work on the evolution of the

Jeanne d'Arc basin of Grand Banks (Kusznir and Egan, 1989) shows that models utilising an elastic thickness of 10 km most closely predict the present subsidence in the basin and observed crustal structure. If these values are correct, Figure 5b suggests that footwall uplift can be between a few tens of metres and 1.5 km following rifting, depending upon the amount of extension. These results agree with investigations of footwall upllift in the geological record. For example, Yielding (1990) assessed the amount of footwall erosion on the tilted fault blocks in the northern North Sea in order to provide constraint upon the magnitude of the original uplift. He proposed footwall erosion to be between 100 m and 1.4 km. Similarly, Weissel and Karner (1989) in their study of continental rifts observed uplifts of the order of 1 km flanking the Gulf of Suez and 1.3 km flanking the Albert rift (East Africa). Hellinger and Sclater (1983) suggested footwall shoulder upwarpings of the Rhine graben of over 1 km, while Jackson and McKenzie (1983) propose footwall uplifts of between 0.5 and 1 km for the Aegean.

The results presented here have been calculated by assuming extension along a single fault with a listric geometry and, as a consequence, care should be taken when applying them to real examples. Extensional basin formation usually occurs by extension along a sequence of basement faults, rather than a single fault structure. This implies that basement geometry, including the magnitude of footwall uplift, will result from the superposition of flexural isostatic deflections caused by extension along each of the faults. There has also been a lot of debate recently as to the geometry of normal faults and, in particular, the validity of major basement faults with a listric geometry. Indeed, seismological investigations of presently active normal faults suggests that they are planar within the brittle seismogenic layer (Jackson and McKenzie, 1983). Although the results in this paper have been calculated in the context of a listric fault, the individual loads and the methodology described for calculating the associated flexural isostatic responses are applicable to other fault geometries. The actual magnitudes of the loads will be different, however, so that the results presented in the figures should only be used as approximations in the context of more complex extensional fault structures.

7. Conclusions

(1) The elastic strength of the lithosphere must be considered when investigating isostatic adjustments occurring in response to the application of a tectonically generated load, such as that arising from crustal thinning by normal faulting.

(2) The extension of the lithosphere can be represented as a fault-controlled (simple shear) process at shallow, brittle depths giving away to a stretching (pure shear) mechanism in deeper ductile regions. During rifting this pattern of extension subjects the lithosphere to a suite of loads. Negative loads result from both simple shear thinning of the crust and the rift-induced elevation of the geothermal gradient. These produce uplift. Positive loading arises from the thinning of the lower crust due to pure shear and the infill of the basin with water and/or sediment. These produce subsidence. Following rifting, the temperature field gradually cools back to its original state over a time period of about 100 Ma and generates a further positive load. The additional subsidence produced by this load is further enhanced by sediment loading.

(3) The combined effect of all of the above loads after flexural isostatic adjustment is to produce a resultant basin with uplift of the flanking footwall shoulder and a smooth fault geometry, while the underlying Moho topography is relatively broad and flat. The sedimentary infill pattern within the basin shows a localised deep component associated with rifting overlain by a broad relatively thin blanket of deposition associated with thermal subsidence.

(4) Extension causes an uplift of the footwall mainly due to flexural isostatic uplift in response to crustal thinning. The magnitude of this uplift is controlled by a combination of the amount of extension, the flexural rigidity of the lithosphere, the dip of the fault along which extension has taken place, basin infill and erosion. Basin depth and Moho topography are also strongly influenced by these parameters.

(5) Footwall uplift is rarely seen on seismic reflection data across many basins due to the effects of erosion. Modelling shows that the erosion of this localised topography induces regional flexural uplift.

(6) The models predict footwall uplift of between a few tens of metres and 1.5 km for realistic amounts of extension and flexural rigidity. These figures correlate closely with the amount of footwall uplift deduced from the geological record.

Acknowledgements

I thank Nick Kusznir and Garry Karner for useful guidance and discussion during the initial stages of this work. The manuscript has benefited from review by Professor M.H.P. Bott.

Appendix

Numerical solution to the calculation of the flexural isostatic response of the lithosphere to loading

In this section the numerical method used for the calculation of the two-dimenional flexural response of the lithosphere to tectonic loading is described. The method is similar to that used in other works on the modelling of lithospheric flexure (e.g. Watts et al., 1982), however, the mathematics are presented in a simplified form so that the theory can be easily understood by the reader.

As described in section 2, the flexural deflection of the lithosphere (w_x) in response to a load (L_x) is given by:

$$\frac{d^2}{dx^2}D\frac{d^2w_x}{dx^2}+(p_m-p_l)gw_x=L_x \tag{A1}$$

where D is flexural rigidity, g is acceleration due to gravity and p_m and p_l are the densities of mantle and load, respectively.

For simplicity, a sinusoidally distributed load is considered initially (after Turcotte and Schubert, 1982):

$$L_x=L_0\sin(2\pi x/\lambda) \tag{A2}$$

where L_0 defines the peak of the load and λ is its wavelength.

Equation A1 shows that the deflection of the lithosphere, w_x, is directly proportional to the applied load, which implies that if the load varies sinusoidally, so must the deflection it produces. Therefore:

$$w_x=w_0\sin(2\pi x/\lambda) \tag{A3}$$

where w_0 is the maximum deflection of the lithosphere. Substituting for w_x into eqn. A1 and simplifying gives:

$$D(2\pi/\lambda)^4w_0+(p_m-p_l)gw_0=L_0 \tag{A4}$$

By rearrangement the maximum deflection of the lithosphere is obtained:

$$w_0=L_0/D(2\pi/\lambda)^4+(p_m-p_l)g \tag{A5}$$

More realistically lithosphere loads are not sinusoidally distributed, but are continually variable. They can be conveniently represented as a series of sine and cosine components combines as a Fourier series:

$$L_x=(b_0/2)+\sum_{n=1}^{\infty}A_n\sin(2\pi nx/s)+B_n\cos(2\pi nx/s) \tag{A6}$$

where b_0, A_n and B_n are the Fourier coefficients such that:

$$b_0=\frac{2}{s}\int_a^b L_x\,dx \tag{A7}$$

$$A_n=\frac{2}{s}\int_a^b L_x\sin(2\pi nx/s)\,dx \tag{A8}$$

$$B_n=\frac{2}{s}\int_a^b L_x\cos(2\pi nx/s)\,dx \tag{A9}$$

where s is the width of the load, b-a.

By incorporating eqn. A5 into the Fourier series, the flexural response of the lithosphere to a varying load can be calculated such that:

$$w_x=(b_0'/2)+\sum_{n=1}^{\infty}[A_n'\sin(2\pi nx/s)]+[B_n'\cos(2\pi nx/s)] \tag{A10}$$

The Fourier coefficients are now modified such that:

$$B_0'=\frac{2}{s}\int_a^b\frac{Lx}{(p_m-p_l)g}dx \tag{A11}$$

$$A_n'=\frac{2}{s}\int_a^b\frac{Lx}{D(2\pi n/s)^4+(p_m-p_l)g}\sin(2\pi nx/s)\,dx \tag{A12}$$

$$B_n'=\frac{2}{s}\int_a^b\frac{L_x}{D(2\pi n/s)^4+(p_m-p_l)g}\cos(2\pi nx/s)\,dx \tag{A13}$$

Equations A10 to A13 can be applied to calculate the flexing of the lithosphere in response to any tectonic load so long as both the magnitude and density of the load are defined correctly (see section 3). The load, which is in reality a continuous function, is represented as a sequence of values an equal sampling interval apart. The results presented here have been calculated using a sampling increment of 5 km, a width of load of 400 km and 50 Fourier components.

References

Airy, G.B., 1855. On the computation of the effect of the attraction of mountain-masses, as disturbing the apparent astronomical latitude of stations in geodetic surveys. Philos. Trans. R. Soc. London, 145: 101–104.

Beaumont, C., 1978. The evolution of sedimentary basins on a viscoelastic lithosphere: theory and examples. Geophys. J.R. Astron. Soc., 55: 471–498.

Beaumont, C., 1981. Foreland basins. Geophys. J.R. Astron. Soc., 65: 291–329.

BIRPS and ECORS, 1986. Deep seismic profiling between England, France and Ireland. J. Geol. Soc. London, 143: 45–52.

Bott, M.H.P., 1976. Formation of sedimentary basins of the graben type by extension of the continental crust. Tectonophysics, 36: 77–86.

Cochran, J.R., 1983. Effects of finite extension times on the development of sedimentary basins. Earth Planet. Sci. Lett., 77: 362–372.

Couzens, T. and Kusznir, N.J., in press. The rift to drift transition and sequence stratigraphy at passive continental margins. In: Tectonics and Seismic Sequence Stratigraphy. Spec. Publ. Geol. Soc.

Egan, S.S., 1988. Rheological, thermal and isostatic constraints on continental lithosphere extension and compression. Ph. D. thesis, Univ. of Keele, UK.

Enachescu, M.E., 1987. Tectonic and structural framework of the northeast Newfoundland continental margin. In: C. Beaumont and A.J. Tankard (Editors), Sedimentary Basins and Basin Forming Mechanisms. Can. Soc. Pet. Geol. Mem. 12: 117–146.

Gibbs, A.D., 1983. Balanced cross-section constructions from seismic sections in areas of extensional tectonics. J. Struct. Geol., 5: 152–160.

Gibbs, A.D., 1984. Structural evolution of extensional basin margins. J. Geol. Soc. London, 141: 609–620.

Hall, J., Brewer, J.A., Matthews, D.H. and Warner, M.R., 1984. Crustal structure across the Caledonides from the WINCH seismic reflection profile: influences on the evolution of the Midland Valley of Scotland. Trans. R. Soc. Edinburgh (Earth Sci.), 75: 97–109.

Heiskanen, W.A. and Vening Meinesz, F.A., 1958. The Earth and its Gravity Field. McGraw-Hill, New York, N.Y.

Hellinger, S.J. and Sclater, J.G., 1983. Some comments on two-layer extensional models for the evolution of sedimentary basins. J. Geophys. Res., 88: 8251–8269.

Jackson, J.A. and McKenzie, D.P., 1983. The geometrical evolution of normal fault systems. J. Struct. Geol., 5: 471–482.

Keen, C.E., Boutilier, R., De Voogd, B., Mudford, B. and Enacheseu, M., 1987. Crustal geometry and models of the evolution of the rift basins on the Grand Banks off eastern Canada: constraints from deep seismic reflection data. In: C. Beaumont and A.J. Tankard (Editors), Sedimentary Basins and Basin Forming Mechanisms. Can. Soc. Pet. Geol. Mem., 12: 101–116.

King, G.C.P., Stein, R.S. and Rundle, J.B., 1988. The growth of geological structures by repeated earthquakes. 1. Conceptual framework. J. Geophys. Res., 93 (B11): 13, 307–13, 318.

Kusznir, N.J. and Egan, S.S., 1989. Simple-shear and pure-shear models of extensional sedimentary basin formation: application to the Jeanne d'Arc basin, Grand Banks of Newfoundland. A.A.P.G. Mem, 46: 305–322.

Kusznir, N.J. and Karner, G.D., 1985. Dependence of the flexural rigidity of the continental lithosphere on rheology and temperature. Nature, 316: 138–142.

Kusznir, N.J. and Park, G., 1987. The extensional strength of the continental lithosphere: its dependence on geothermal gradient, crustal composition and thickness. In: M.P. Coward, J.F. Dewey and P.L. Hancock (Editors), Continental Extensional Tectonics. Geol. Soc. London Spec. Publ., 28: 35–52.

Kusznir, N.J., Karner, G.D. and Egan, S.S., 1987. Geometric, thermal and isostatic consequences of detachments in continental lithosphere extension and basin formation. In: C. Beaumont and A.J. Tankard, (Editors), Sedimentary Basins and Basin Forming Mechanisms. Can. Soc. Pet. Geol. Mem., 12: 185–203.

Kusznir, N.J., Marsden, G. and Egan, S.S., 1991. Flexural cantilever simple-shear/pure-shear model of continental lithosphere extension: application to the Jeanne d'Arc basin, Grand Banks and Viking Graben, North Sea. Geol. Soc. London Spec. Publ., 56: 41–60.

Marsden, G., Yielding, G., Roberts, A.M. and Kusznir, N.J., 1990. Application of a flexural cantilever simple-shear/pure shear model of continental lithosphere extension to the formation of the northern North Sea basin. In: D.J. Blundell and A.D. Gibbs, (Editors), Tectonic Evolution of the North Sea Rifts. Oxford University Press London, pp. 236–257.

McKenzie, D.P., 1978. Some remarks on the development of sedimentary basins. Earth Planet. Sci. Lett., 40: 25–32.

Royden, L. and Keen, C.E., 1980. Rifting processes and thermal evolution of the continental margin of eastern Canada determined from subsidence curves. Earth Planet. Sci. Lett., 51: 343–361.

Tankard, A.J. and Welsink, H.J., 1987. Extension tectonics and stratigraphy of the Mesozoic Grand Banks of Newfoundland. In: W. Manspeizer (Editor), Triassic–Jurassic Rifting and the Opening of the Atlantic Ocean. Elsevier, Amsterdam.

Tankard, A.J., Welsink, H.J. and Jenkins, W.A.M., 1989. Structural styles and stratigraphy of the Jeanne d'Arc basin, Grand Banks of Newfoundland. A.A.P.G Mem., 46: 265–282.

Turcotte, D.L., 1979. Flexure, Advances in Geophysics. Academic Press, New York, N.Y.

Turcotte, D.L. and Schubert, G., 1982. Geodynamics: Applications of Continuum Physics to Geological Problems. Wiley, New York, N.Y., 450 pp.

Vening Meinesz, F.A. 1950. Les Graben africains, resultat de compression ou de tension dans la croute terrestre. Bull. Inst. R. Colon. Belg., 21: 539–552.

Verall, P., 1982. Structural interpretation with applications to North Sea problems. JAPEC, Course Notes No. 3.

Walcott, R.I., 1970. Flexural rigidity, thickness and viscosity of the lithosphere. J. Geophys. Res., 75: 3941–3954.

Watts, A.B., Karner, G.D. and Steckler, M.S. 1982. Litho-

spheric flexure and the evolution of sedimentary basins. In: P. Kent, M.H.P. Bott, D.P. McKenzie and C.A. Williams, (Editors), The Evolution of Sedimentary Basins. Philos. Trans. R. Soc. London, Ser. A, 305: 249–281.

Weissel, J.K. and Karner, G.D., 1989. Flexural uplift of rift flanks due to tectonic denudation of the lithosphere during extension. J. Geophys. Res., 94: 13, 919–13, 950.

Wernicke, B. and Burchfiel, B.C., 1982. Modes of extensional tectonics. J. Struct. Geol., 4: 105–115.

White, N.J., Jackson, J.A. and McKenzie, D.P., 1986. The relationship between the geometry of normal faults and that of sedimentary layers in their hangingwalls. J. Struct. Geol, 8: 897–910.

White, N. and McKenzie, D., 1988. Formation of the "steer's head" geometry of sedimentary basins by differential stretching of the crust and mantle. Geology, 16: 250–253.

Yielding, G., 1990. Footwall uplift associated with Late Jurassic normal faulting in the northern North Sea. J. Geol. Soc., London, 147: 219–222.